Wintertime Polynya Structure and Variability From Thermal Remote Sensing and Seal-Borne Observations at Pine Island Glacier, West Antarctica

Elena Savidge, Tasha Snow, Matthew R. Siegfried, *Member, IEEE*, Yixi Zheng, Ana B. Villas Bôas, Guilherme A. Bortolotto, Lars Boehme, and Karen E. Alley

***Abstract*— Antarctica's ice shelves play a critical role in modulating ice loss to the ocean by buttressing grounded ice upstream. With the potential to impact ice-shelf stability, persistent polynyas (open-water areas surrounded by sea ice that occur across multiple years at the same location) at the edge of many ice-shelf fronts are maintained by winds and/or ocean heat and are locations of strong ice–ocean–atmosphere interactions. However, in situ observations of polynyas are sparse due to the logistical constraints of collecting Antarctic field measurements. Here, we used wintertime (May–August) temperature and salinity observations derived from seal-borne instruments deployed in 2014, 2019, and 2020, in conjunction with thermal imagery from the Moderate Resolution Imaging Spectroradiometer (MODIS) and the Landsat 8 Thermal Infrared Sensor (TIRS) to investigate spatial, temporal, and thermal structural variability of polynyas near Pine Island Glacier (PIG). Across the three winters considered, there were 176 anomalously warm (>3σ from background) seal dives near the PIG ice front, including 26 dives that coincided with MODIS images with minimal cloud cover that also showed a warm surface temperature anomaly. These warm surface temperatures correlated with ocean temperatures down to 150 m depth or deeper, depending on the year, suggesting that MODIS-derived surface thermal anomalies can be used for monitoring polynya presence and structure during polar night. The finer spatial resolution (100 m) of TIRS wintertime thermal imagery captures more detailed thermal structural variability within these polynyas, which may provide year-round insight into subice-shelf processes if this dataset is collected operationally.**

***Index Terms*— Ice-ocean interaction, Landsat 8 Thermal Infrared Sensor (TIRS), Moderate Resolution Imaging Spectroradiometer (MODIS), persistent polynyas, thermal remote sensing.**

Manuscript received 8 September 2022; revised 9 December 2022 and 20 March 2023; accepted 25 March 2023. Date of publication 28 April 2023; date of current version 17 May 2023. This work was supported in part by the National Science Foundation - Natural Environment Research Council (NSF-NERC) International Thwaites Glacier Collaboration: Thwaites-Amundsen Regional Survey and Network (ITGC: TARSAN) under grant NE/S006419/1 (NERC), grant NE/S00659/1 (NERC), and grant 1738992 (NSF); and in part by the NERC Ice Sheet Stability Programme (iSTAR) under grant NE/J005703/1. The work of Elena Savidge was supported in part by the Doctoral NSERC Award under grant 557347 and in part by the NASA Cryospheric Science Program under grant 80NSSC22K0385. The work of Tasha Snow was supported in part by the NASA Cryospheric Science Program under grant 80NSSC22K0385 and in part by the NASA Earth and Space Science Fellowship Program under grant NNX16AO33H. The work of Matthew R. Siegfried was supported by the NASA Cryospheric Science Program under grant 80NSSC22K0385. The work of Yixi Zheng was supported in part by the China Scholarship Council, in part by the University of East Anglia, in part by the European Research Council (under H2020-EU.1.1.) under grant 741120: COMPASS, and in part by the NERC Research Grant under grant NE/W007045/1 NSF Directorate for Geosciences (NSFGEO)-NERC: Collaborative Research: ARTEMIS. The work of Ana B. Villas Bôas was supported in part by the NASA Cryospheric Science Program under grant 80NSSC22K0385 and in part by the NASA S-MODE Program under grant 80NSSC19K1004. The work of Karen E. Alley was supported by NSERC under grant RGPIN-2021-02910. *(Corresponding author: Elena Savidge.)*

This work involved human subjects or animals in its research. Approval of all ethical and experimental procedures and protocols was granted by Foreign & Commonwealth Office/United Kingdom Permit #29/2018.

Elena Savidge, Tasha Snow, Matthew R. Siegfried, and Ana B. Villas Bôas are with the Department of Geophysics, Colorado School of Mines, Golden, CO 80401 USA (e-mail: esavidge@mines.edu; tsnow@mines.edu; siegfried@mines.edu; villasboas@mines.edu).

Yixi Zheng is with the School of Environmental Science, University of East Anglia, NR4 7TJ Norwich, U.K. (e-mail: yixi.zheng@uea.ac.uk).

Guilherme A. Bortolotto and Lars Boehme are with the School of Biology, University of St Andrews, KY16 9TH St Andrews, U.K. (e-mail: abdo@st-andrews.ac.uk; lb284@st-andrews.ac.uk).

Karen E. Alley is with the Department of Environment and Geography, University of Manitoba, Winnipeg, MB R3T 2N2, Canada (e-mail: karen.alley@umanitoba.ca).

This article has supplementary downloadable material available at https://doi.org/10.1109/TGRS.2023.3271453, provided by the authors.

Digital Object Identifier 10.1109/TGRS.2023.3271453

I. Introduction

PINE Island Glacier (PIG) is one of the fastest flowing outlet glaciers in West Antarctica [1], [2], and drains 10% of the West Antarctic Ice Sheet (WAIS) [3]. In the past decade, PIG has experienced rapid acceleration, grounding line retreat, and ocean-driven thinning, increasing its contribution to sea level rise [1], [2], [4]. This increase in dynamic ice-mass loss has largely been driven by inflows of warm modified Circumpolar Deep Water (mCDW) [5], [6], [7], an ocean water mass characterized by temperatures typically >0 °C, absolute salinities >34.7 g/kg, and depths below ∼350 m (see [7], [8], [9]). mCDW reaches the continental shelf via bathymetric troughs (see [10]) and can circulate beneath PIG ice shelf (PIGIS), the portion of the glacier floating on the ocean.

Circulation of mCDW beneath PIGIS reaches the grounding zone (the region where grounded ice transitions to ice shelf), and the depth at which it subsequently exits the cavity can vary seasonally. Depending on their buoyancy, plumes may flow out of the subice-shelf cavity and into Pine Island Bay (PIB) at depths that coincide with the base of the ice shelf (∼200–400 m depending on local ice thickness; see [11], [12]) or they may rise to the surface [13]. The depth at which plumes exit the subice-shelf cavity depends on upper ocean (less than ∼450-m depth) density and stratification, which vary

seasonally. In wintertime, the homogeneous mixed layer is relatively dense due to surface cooling and brine rejection and can extend from the surface down to as deep as ∼400 m on the Amundsen Sea continental shelf [14], allowing more frequent surfacing of meltwater (MW) plumes than in summertime [13]. In summertime, the upper ocean is strongly stratified, causing plumes to spread along isopycnals rather than rising to the surface [13], [15].

The warm, buoyant, MW-rich plumes can incise inverted channels at the base of the ice shelf, called basal channels [16], [17], [18], which provide pathways that concentrate warm buoyant water from the grounding zone toward ice shelf fronts. Depending on basal channel outflow strength and on upper ocean density, buoyant plumes sometimes reach the surface where they can melt sea ice and generate open-water areas (or intermittently thin sea ice areas) surrounded by thicker sea ice, called sensible-heat polynyas. Alternatively, polynyas can also be mechanically opened and maintained by off-shore winds pushing sea ice away from the ice front/coast called latent-heat polynyas; these are linear in shape and typically follow coastline orientation compared to the near-circular sensible-heat polynyas. Polynya formation mechanisms (i.e., ocean heat and wind forcing) are not mutually exclusive, meaning both polynya types can coexist at the same time and place [19]. Sensible-heat polynyas often form in the same location for multiple years (i.e., persistent polynyas) and are collocated with shear margins or subice-shelf channel outlets for ice shelves with cavities flooded by relatively warm water (i.e., warm-cavity ice shelves) [16], [17], suggesting that basal channels are likely intrinsically related to polynya formation processes. Furthermore, basal channels are important ice-shelf features that substantially change basal melt patterns (see [20], [21]) and may influence ice shelf stability through fracture [22], particularly when channels occur in already-weak shear margins [17], as is the case for PIG. However, basal channel, plume, and polynya variability and coevolution remain relatively unexplored.

Persistent polynyas are key sites of consistent, year-round interactions between atmosphere, sea ice, ocean, ice shelves, and subice-shelf ocean cavities that drive Southern Ocean carbon dynamics [23], [24]; however, in situ observations are sparse due to the logistical constraints of collecting field measurements given the remoteness of Antarctica [25]. Instead, visible (see [16], [26]), thermal (see [27], [28]), and microwave (see [29], [30]) remote sensing techniques have been used to identify and quantify polynya processes in coastal Antarctica. Although multiple remote sensing techniques can identify the presence of polynyas within sea ice, thermal remote sensing, with spatial resolution ∼10–25 times finer than passive microwave [31], has the unique potential to fingerprint regions of high sea surface temperatures within PIB, which can be used to infer processes that govern sensible-heat polynya evolution. For example, warm thermal anomalies were consistently identified in summertime at the PIGIS front, where both persistent polynyas and strong basal outflow occur [18], [32]. However, although satellite thermal infrared measurements are spatially extensive, they only measure the temperature of the upper ∼10 μm of the ocean [33].

Here we used thermal infrared satellite imagery from the Moderate Resolution Imaging Spectroradiometer (MODIS) and Landsat 8 Thermal Infrared Sensor (TIRS) combined with seal-borne hydrographic ground-truth measurements to study wintertime polynya processes at PIG. Recently, seal-borne oceanic measurements in the Amundsen Sea have provided a substantial hydrographic dataset [14] that allows for both wintertime (when sea ice is more extensive) and more frequent observations than are available via ship-borne methods (largely limited to sea ice-free conditions). These seal-derived hydrographic data provide some of the first vertical measurements of polynya/plume structure in the Antarctic (see [13]). Therefore, combining these remote sensing and in situ datasets allows for a more comprehensive understanding of how polynya processes evolve year-round. Coupling these datasets, we found that MODIS thermal anomalies can be used for monitoring polynya structure and evolution during polar night and that the finer spatial resolution (100 m) of Landsat 8 wintertime thermal imagery captures detailed thermal structural variability within these polynyas, which may provide insight into subice-shelf processes during polar night if these scenes are collected operationally. Acquiring high resolution wintertime ocean thermal measurements near Antarctica's ice shelves in polar winter is crucial for our year-round understanding of polynya and frontal processes. This effort becomes particularly important when ocean field records are sparse, as is often the case in Antarctica.

II. Methods

A. Datasets

1) MODIS Thermal Data: We used MODIS Level 2 Atmospherically Corrected Surface Reflectance thermal data (MOD/MYD09 Band 31; 10.780–11.280 μm) from the MODIS instrument operating on NASA Aqua (MYD) and Terra (MOD) satellites to investigate the sensible-heat polynyas near the PIG ice front. We use MOD09 brightness temperature in lieu of absolute temperatures because sea surface temperatures are particularly difficult to retrieve in polar regions (see [34]). The temperatures we provide have not been corrected for surface emissivity; however, the thermal infrared emissivity of ocean water is close to that of a blackbody so this correction would not substantially change the temperatures we provide here. MODIS thermal images are taken at high temporal resolution at the Earth's poles (>10 per day), making them ideal for monitoring the temporal evolution of sensible-heat polynyas; however only 1–3 wintertime images per day are processed into the MOD/MYD09 datasets due to errors arising from cloud shadow, high aerosol content, high view angle, or high solar zenith angle [35]. The spatial resolution of MODIS thermal images ranges from 1-km pixels directly at nadir to ∼4 km at the across-track edges of the footprint. As polynyas at PIG can be several kilometers across, we investigated whether MODIS data are adequate to monitor the spatial evolution of polynyas. We selected all of the MODIS thermal images obtained between May and August (constrained to these months to match the time period of wintertime seal-tag data availability near PIGIS) of 2014,

2019, and 2020 that contained minimal dense cloud coverage; due to the difficulty of implementing effective cloud filtering algorithms during polar night (see [36], [37]), we selected only images where surface features were clearly defined in the thermal imagery, which indicated that clouds were at a minimum. We performed this step manually on a scene-by-scene basis.

2) Landsat 8 Thermal Data: We used Landsat 8 Collection 2 Level 1 Systematic Terrain Correction (L1GT) Band 10 (10.6–11.19 μm) imagery acquired during the 2019 austral winter to investigate the sensible-heat polynya signal at a finer spatial resolution. L1GT is a brightness temperature product (i.e., not calibrated surface temperature) as there is currently no calibrated sea surface temperature product from Landsat [38]. Landsat 8 does not operationally collect data during polar night, and so this austral winter dataset was collected through a data acquisition special request. Landsat 8 thermal bands have much finer spatial resolution (100 m) than MODIS thermal bands (1 km), but, during operational data collection, have lower temporal resolution (one scene collected every 3–5 days).

3) Seal-Borne Oceanographic Data: We used temperature and salinity profiles measured during austral winter (May to August) by seal-borne conductivity-temperature-depth-satellite relayed data loggers (CTD-SRDLs) deployed in 2014, 2019, and 2020 [39]. Although limited reference data in remote locations may degrade data quality slightly [40], each CTD-SRDL recorded ocean temperature and salinity with an accuracy better than 0.005 °C and 0.02 (using the practical salinity scale), respectively, making seal-tag measurements a reliable means of collecting hydrographic data. CTD-SRDLs were temporarily attached to a seal's head and recorded conductivity, temperature, and pressure at 1 Hz [40] across the Amundsen Sea (a region >100 000 km^2). Seal positions estimated to be inland were adjusted using standard repositioning algorithms (see the Supplementary Material for method). Onboard processing reduced each dive profile into 17 or 18 depth levels following the methods of [13]. This data reduction step was meant to maximize data retention where the largest vertical conductivity and temperature gradients occur in the water column and to minimize data volume to transfer via the bandwidth-limited Argos satellite-communication system [40]. Only the deepest dive within every four-hour period was transmitted to ensure the best possible spatial and temporal resolution for the limited battery power available [40]. For each CTD profile, we vertically interpolated the data to 1 m intervals using a piecewise cubic hermite interpolating polynomial [42].

The 2014 hydrographic dataset was collected by 14 seals tagged with CTD-SRDLs during the UK's Ice Sheet Stability Program (iSTAR) JR294/295 cruise in February 2014 onboard the RRS James Clark Ross [14]. Hydrographic datasets in 2019 (12 tagged seals) and 2020 (12 tagged seals) were collected with similar methods during cruises NBP19-02 and NBP20-02 onboard the RVIB Nathaniel B. Palmer [43], as part of the International Thwaites Glacier Collaboration: Thwaites-Amundsen Regional Survey and Network (ITGC: TARSAN).

B. Data Processing

1) Polynya and Background Profile Partitioning: Hydrographic profile measurements that sample sensible-heat polynyas record warmer near-surface ocean temperatures than those that do not [13], [18]. We therefore statistically partitioned "warm" polynya profiles and "background" profiles to detect polynyas based on the ocean temperature in the upper 20 m of the water column, where we have dense CTD sampling despite the inherent vertical data reduction that occurs for each profile (see Figs. S1 and S2). We estimated an annual wintertime-mean background surface temperature and standard deviation using May–August upper 20 m ocean temperatures in the center of PIB (pink dashed box in Fig. 1), excluding profiles directly adjacent to or west of the ice front, where warm plumes commonly impact surface temperatures [13], [18], [32]. Capturing annual wintertime-means ensures that we account for interannual temperature variability in PIB. We used three standard deviations warmer than mean annual background surface (i.e., upper 20 m) ocean temperatures as a threshold for delineating warm polynya profiles, and labeled the remaining profiles as background. This method therefore defines warm polynya profiles where surface temperatures are warmer than 99% of the background surface temperatures.

2) Meltwater Content: We followed the method presented in [13] to calculate MW content from seal-tag hydrographic profiles. This method infers the fraction of glacial MW at each observed location assuming the ocean in this region is composed of a linear mixture of the three wintertime PIB water masses (mCDW, Winter Water [WW], and MW). We used conservative temperature, Θ, and absolute salinity, S_A, as end-members and assumed they are both conservative. We determined the mCDW endpoints for each year by extracting the maximum seal-derived Θ and S_A that fall within an expected range for mCDW in PIB (i.e., $S_A > 34.7$ g/kg and $\Theta > 0.5$ °C) from all May to August seal-tag data. WW is formed in the winter due to strong winds, sea ice formation, and surface cooling and always has a temperature near the in situ freezing point (~ -1.86 °C [13], [44]); therefore, we determined the WW S_A endpoints for each year by extracting the highest observed salinity that lies on the freezing line (where $\Theta = -1.86$ °C). We used MW endpoints from [13].

Uncertainty in the endpoints may be as much as 30% of the averaged wintertime near-surface MW content due to seal-tag hydrographic measurement uncertainties [13]. Our seal-tag data captured stable wintertime mCDW properties, so errors originating from the mCDW endpoint selection are negligible. Following [13], we estimated the error in the WW S_A endpoint to be $\pm$ 1.1 g/kg using a Monte Carlo simulation on a set of 1000 randomly generated hydrographic measurements (with criteria: $\Theta > -1.9$ °C and MW content >25 g/kg) with 2000 different WW endpoints (normally distributed around 34.21 $\pm$ 0.05 g/kg). If the above procedure is replicated, these uncertainties may change the values of the calculated MW content we present, but no qualitative change should be expected because the uncertainties calculated are much lower than the difference found between the background and warm profile MW content (see Section III-C).

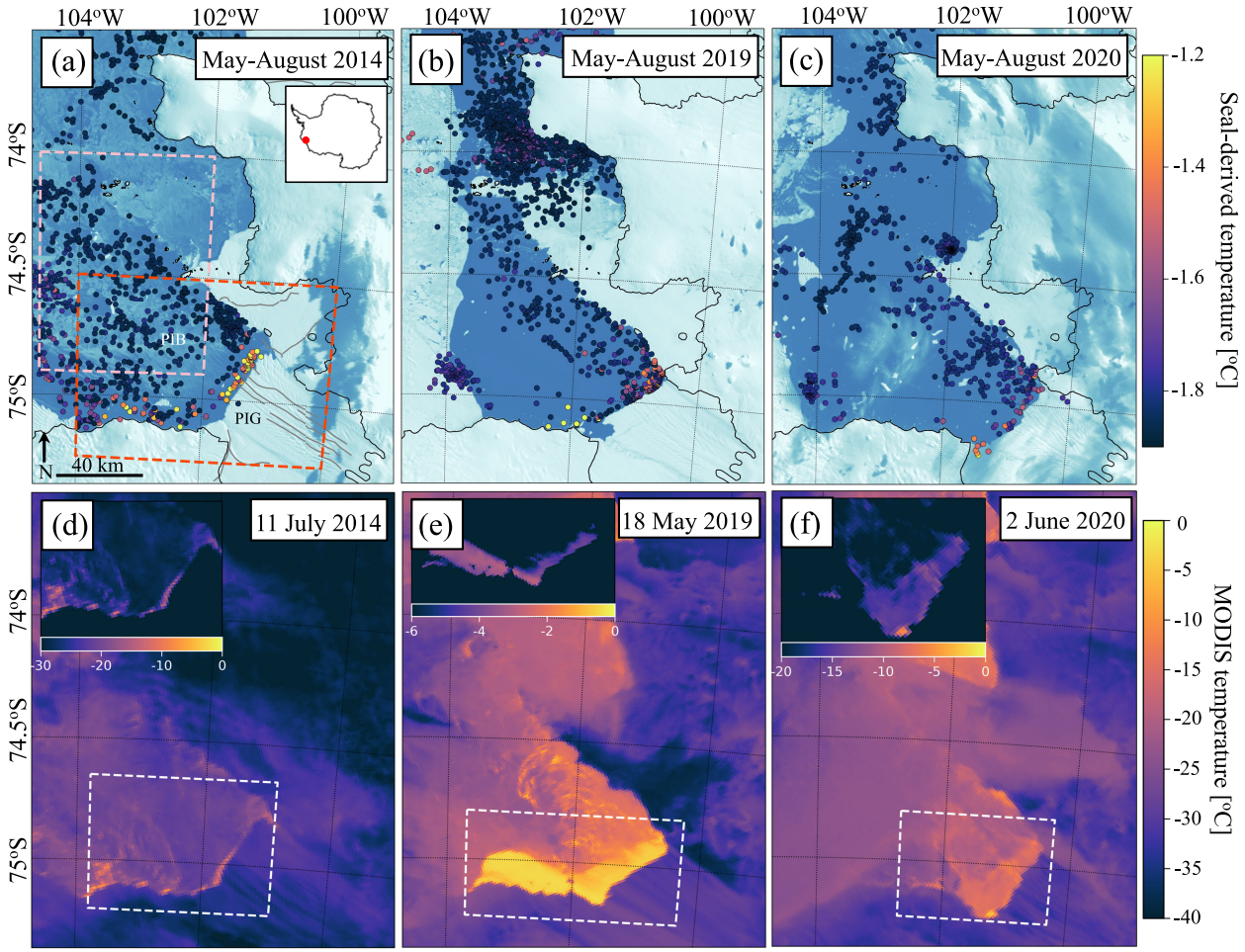

Fig. 1. (a) 2014, (b) 2019, and (c) 2020 distribution of May to August seal-tag-derived mean temperature for the upper 20 m of the water column. The grounding line [46] is marked by a thin black line. Basal channels [16] are marked by gray lines in (a). Dashed orange bounding box in (a) indicates our study area. Pink dashed box in (a) represents the area in which we calculated background seal-tag-derived surface temperatures, excluding warm thermal anomalies. Selected MODIS thermal images from (d) July 11, 2014, (e) May 18, 2019, and (f) June 2, 2020 show relatively warm surface temperatures near the PIG ice front. Insets show the polynya area (dashed white box) with a linear colormap stretch applied to highlight detail.

3) Surface-Subsurface Water-Column Correlations: Following [45], we used seal-derived temperature fields to investigate to what extent surface temperature data could be used for characterizing subsurface ocean temperatures. We quantified the depth at which subsurface temperatures decorrelated from the surface layer for each warm profile by comparing seal-derived mean temperatures at 50 m depth intervals down to 300 m (e.g., $T_{50–100}$ corresponds to the mean temperature within the 50–100 m layer) to the upper 50 m mean temperature, $T_{0–50}$. We estimated correlations between near-surface ($T_{0–50}$) and mixed-layer temperatures at each depth interval and identified all statistically significant ($p < 0.05$) correlations.

III. Results

A. MODIS Observations

In all three winters, we observed relatively warm surface temperatures (up to −3.0 °C) near the PIG ice front [see Fig. 1(d)–(f)]. These warm areas appear as either circular features or linear features following coastline orientation. The circular/subcircular surface temperature anomalies (∼1 to >8 km in diameter, 1 °C to 10 °C warmer than mean surface temperature) are collocated with known locations of basal channels [16]. Therefore, we followed existing literature (see [16], [17], [18]) and attributed these surface temperature anomalies to sensible-heat polynyas. Relatively warm surface temperature anomalies that cross the entire PIGIS calving front (∼1 to >20 km in width; see Fig. 2) were attributed to latent-heat polynyas; MODIS observations showed that latent-heat polynyas can open quickly (hours to days) and that overlapping sensible- and latent-heat polynyas can be distinguished based on the magnitude of the thermal anomaly (see Fig. 2). The warmest wintertime surface temperatures were almost always recorded near the western shear margin, and sometimes also appeared near the middle and eastern shear margin of PIGIS where basal channel outflow has previously been identified [16], [18], [32].

B. Landsat Observations

There were 58 TIRS scenes that covered the PIGIS front from May 2019 to August 2019. We show two of these scenes that overlapped with MODIS imagery (where cloud cover was minimal in both TIRS and MODIS scenes) and that coincided

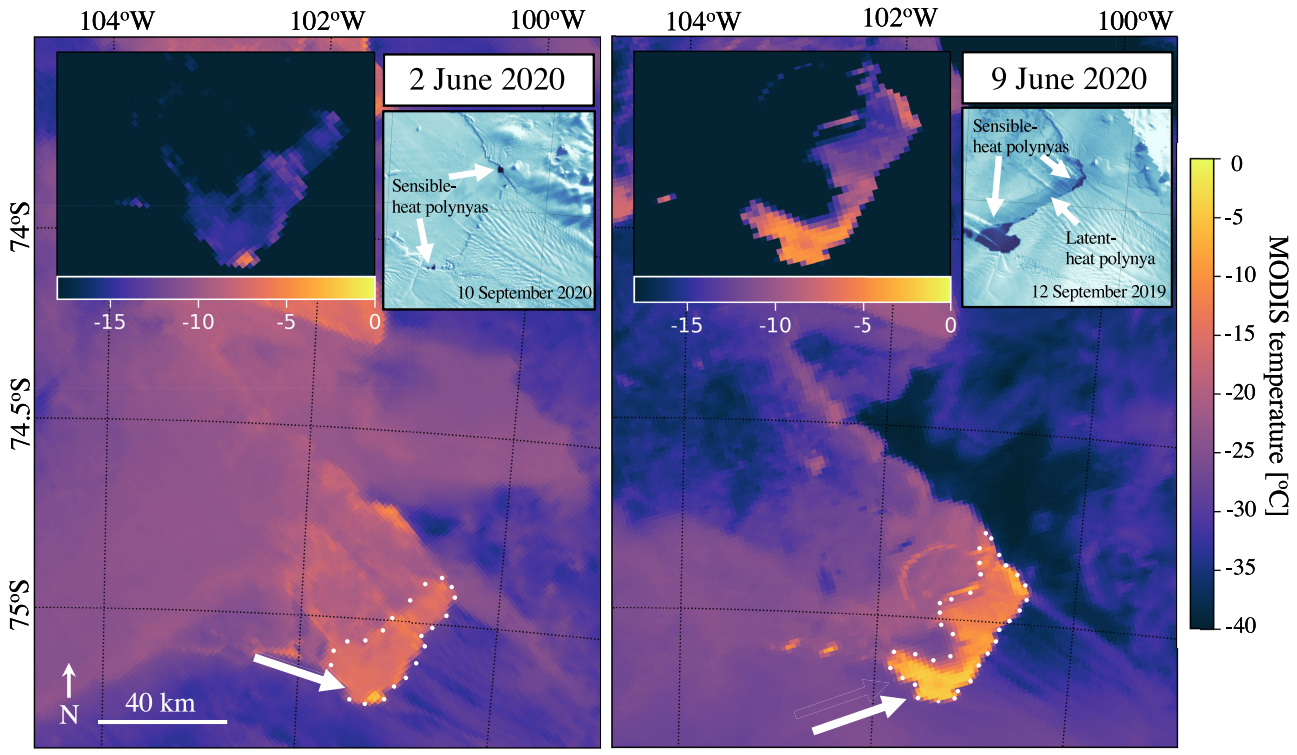

Fig. 2. Evolution of latent- (across entire calving front; indicated by the white dotted polygons) and sensible- (warmest near-circular anomaly near the western shear margin; indicated by the white arrows) heat polynyas from MODIS imagery near PIGIS over a seven-day period in June 2020. MODIS captures the evolution of the western shear margin sensible-heat polynya over this seven-day period. MODIS visible imagery insets show sea ice conditions on September 10, 2020 and September 12, 2019 to demonstrate examples of sensible- and latent-heat polynyas (here intermittently covered by rapidly forming thin sea ice) in optical bands. Exact temporal comparison between optical and thermal images is not possible as thermal images are taken in polar night.

with seal-borne measurements (see Fig. 3). Consistent with MODIS observations, we observed warm TIRS brightness temperature anomalies near the PIG ice front with the warmest signal occurring near the western shear margin. The warm signal near the western shear margin often extended west of the shear margin and paralleled the coast (see Fig. 3, red dotted box), consistent with surface current flow estimates (see [47]). The finer spatial resolution of TIRS imagery (100 m) revealed a more detailed picture of ocean-surface thermal variability, including a cluster of warmer pixels near the middle of the ice front on May 27, 2019 (see Fig. 3, white arrow), located near where a persistent polynya has previously been observed (see [18], [32]). Darker linear features and textured circular areas are visible on the May 27, 2019 imagery (see Fig. 3, orange arrows) and are consistent with types of sea ice that occur early in the ice-formation process (e.g., grease ice, pancake ice; see [48]).

The difference in the time of acquisition between MODIS and TIRS scenes (9 h 10 min difference on May 25; 7 h 33 min difference on May 27) resulted in spatial differences in the thermal data. On May 25 for example, the width of the latent-heat polynya is ~8 km wider in the MODIS scene than in the TIRS scene taken ~9 h later [see Fig. 3 (top row)], indicating that the polynya opened at a rate of ~0.9 km/h. These spatial differences arise because the TIRS image was taken earlier on (7:15 A.M. UTC) in the opening of the latent heat polynya (i.e., sooner after the onset of offshore winds), relative to the MODIS image (4:25 P.M. UTC). Cloud presence also creates thermal variability between scenes.

C. Seal-Derived Observations

We used a total of 1229 CTD profiles collected during seal dives in wintertime near the front of PIG [see Fig. 1(a), orange box]. Applying our profile-partitioning statistical method, we found 462, 325, and 261 background profiles in 2014, 2019, and 2020, respectively. From these profiles, the calculated temperature thresholds that partition warm profiles from background profiles were found to be −1.54 °C, −1.69 °C, and −1.74 °C for each respective year. This thresholding resulted in 66, 72, and 38 warm profiles in 2014, 2019, and 2020, respectively.

We determined Θ and S_A endpoints for mCDW and WW for each year following our MW content calculation method (see Table I). We were unable to calculate the 2020 WW endpoint because no hydrographic data captured conditions near the PIGIS front with temperatures at the freezing point that year; we used the 2019 WW S_A endpoint instead. Using these water mass endmembers, we calculated the wintertime MW content in each year (see Fig. 4).

In all months where we had multiple warm profiles near the front (N_{warm} = 7–50 per month), there was a consistent relationship between temperature and calculated MW: warm profiles corresponded to greater MW content relative to the background profiles in the upper ~300 m (see Figs. 5 and 6). This temperature–MW relationship is consistent with the observations in [13], which were made for 2014 only. The difference in temperature and in MW content between background and warm profiles was usually greatest near the surface

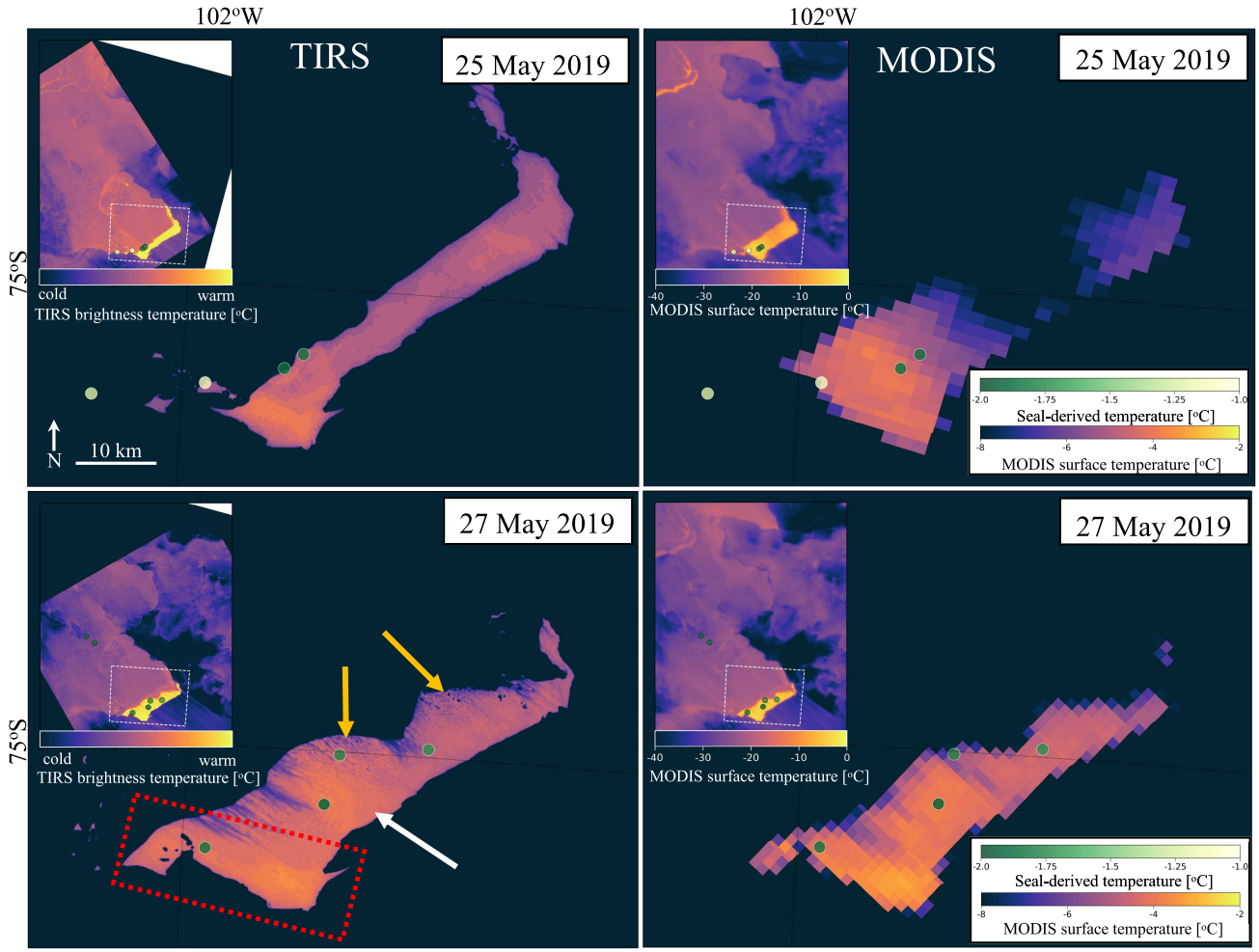

Fig. 3. Comparison of polynya spatial and thermal structure on two days in May 2019 from (Left column) Landsat 8 TIRS and (Right column) MODIS. TIRS (100 m resolution) captures finer-scale detail in comparison to MODIS (1 km resolution). Corresponding seal-derived surface temperatures are overlaid for each day. Mismatch between MODIS- and seal-tag-derived absolute surface temperature retrievals is discussed further in Sections III-D and IV-C. Each panel shows the area within the white dashed box on each inset on a narrower temperature scale to highlight the thermal structure within the latent- and sensible-heat polynyas. The red dotted box highlights relatively warm ocean surface temperatures that often extend west of the western shear margin parallel to the coast and are consistent with surface current flow estimates (see [47]). The white arrow indicates warmer surface temperatures near the middle of the ice front, where strong basal channel outflow has been previously identified [16], [18], [32]. The orange arrows indicate linear features and circular textured areas, consistent with types of sea ice present early in the ice-formation process.

(on average 0.4 °C and 5.4 g/kg, respectively) and decreased through the water column until the water column becomes more homogeneous at depth, dominated by mCDW.

The depth interval at which ocean surface temperatures were significantly ($p < 0.05$) correlated with temperatures at depth varied between years (see Fig. 7). Surface temperatures were correlated with subsurface temperatures down to 150 m depth in 2014 and to 200 m depth in 2019 and 2020 (see Table II) Although these surface-subsurface correlations were statistically significant ($p < 0.05$), they were sometimes weak ($R^2 < 0.3$), suggesting that only the 50–100 m layer was both significantly and strongly (e.g., $R^2 > 0.55$) correlated with the surface layer in 2014 and 2019, for example.

D. Overlapping Seal-Borne and Remote Sensing Observations

Of the 176 anomalously warm profiles near the PIGIS front during the three winters, 26 profiles (across 11 days) coincided with MODIS images with minimal cloud cover. In all 26 cases, a thermal anomaly was present near the PIGIS front when in situ measurements revealed warm surface water. We compared the seal-tag-derived surface temperatures to the warmest MODIS surface temperature within 6 km of each seal dive. We selected a 6 km distance threshold so that the threshold was greater than one MODIS pixel and extracted the warmest temperature within the threshold. This process

TABLE I

ENDMEMBER WATER MASS CONSERVATIVE TEMPERATURE (Θ) AND ABSOLUTE SALINITY (S_A) VALUES FOR ALL YEARS

Year	mCDW	WW	MW
2014	$\Theta = 1.14$ °C $S_A = 34.89$ g/kg	$\Theta = -1.86$ °C $S_A = 34.32$ g/kg	$\Theta = -90.8$ °C $S_A = 0$ g/kg
2019	$\Theta = 0.99$ °C $S_A = 34.91$ g/kg	$\Theta = -1.86$ °C $S_A = 34.21$ g/kg	$\Theta = -90.8$ °C $S_A = 0$ g/kg
2020	$\Theta = 1.03$ °C $S_A = 34.92$ g/kg	$\Theta = -1.86$ °C $S_A = 34.21$ g/kg	$\Theta = -90.8$ °C $S_A = 0$ g/kg

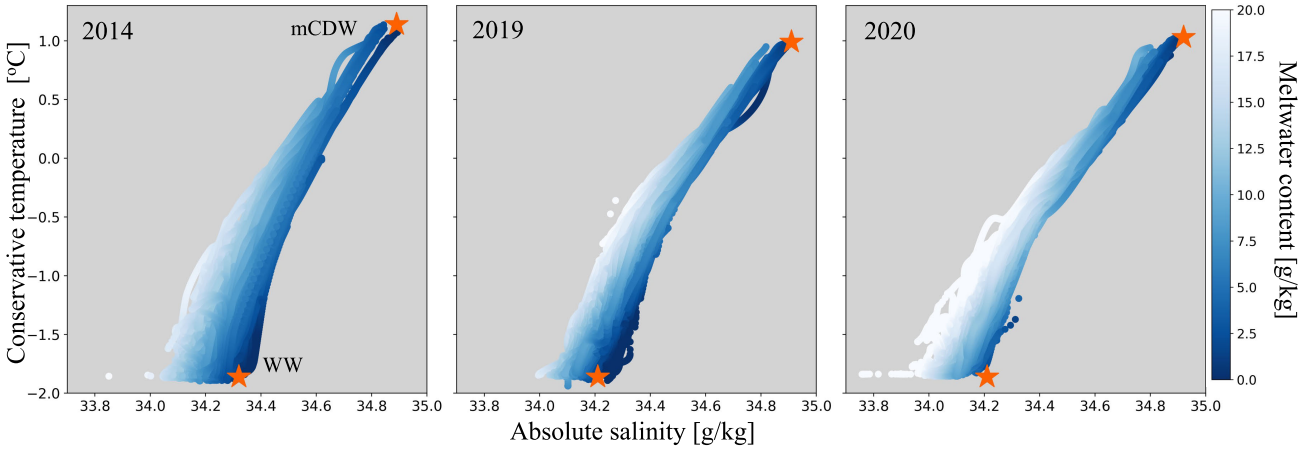

Fig. 4. May–August seal-tag CTD data plotted in temperature-salinity space for each year, colored by MW content. Endmember water properties for mCDW and WW used in the MW calculations are shown with orange stars.

TABLE II

R^2 AND p VALUES (p-VALUES IN PARENTHESES) BETWEEN SURFACE (0–50 m) MEAN SEAL-DERIVED TEMPERATURES AND MEAN TEMPERATURES AT 50 m DEPTH INTERVALS FOR WARM PROFILES IN WINTERTIME. SIGNIFICANT CORRELATIONS ($p < 0.05$) ARE INDICATED IN BOLD. THE EQUIVALENT TABLE FOR BACKGROUND PROFILES CAN BE FOUND IN THE SUPPLEMENTARY MATERIAL (SEE TABLE S1)

	$T_{0-50\ m}$ 2014	$T_{0-50\ m}$ 2019	$T_{0-50\ m}$ 2020
$T_{50-100\ m}$	**0.58 (< 0.001)**	**0.69 (< 0.001)**	**0.55 (< 0.001)**
$T_{100-150\ m}$	**0.15 (0.0018)**	**0.28 (< 0.001)**	**0.40 (< 0.001)**
$T_{150-200\ m}$	0.0097 (0.45)	**0.13 (0.0029)**	**0.12 (0.041)**
$T_{200-250\ m}$	0.0089 (0.47)	0.00012 (0.93)	0.0077 (0.11)
$T_{250-300\ m}$	0.012 (0.39)	0.023 (0.22)	0.0095 (0.58)

ensured that we extracted the closest temperature to that of the ocean given that each pixel may represent a mixture of (relatively warm) sea surface temperature and (cold) cloud or sea ice temperature due to the surface heterogeneity at polynya edges; we also tested thresholds between 5 and 7 km, which did not substantially change our results. However, we found no clear correlation between the extracted MODIS- and seal-tag-derived surface ocean temperatures when performing this comparison between datasets (see Fig. 8). The extracted MODIS temperatures have a much larger range (42 °C) than that of the seal-tag-derived surface temperatures (1.1 °C) for the same days and sampling locations (±6 km). Additionally, across all 26 data pairs, the warmest extracted MODIS temperature is −3.0 °C, whereas seal-tag data record surface ocean temperatures ranging from −1.9 °C to 1.1 °C in this region, indicating discrepancies between the two datasets.

IV. DISCUSSION

A. Remote Sensing Identification of Polynyas

By combining seal-tag-derived anomalously warm surface ocean temperatures and remotely-sensed surface temperature anomalies, we showed that MODIS and TIRS can be used to identify and monitor sensible-heat polynyas near the PIGIS in wintertime. We found that both MODIS and TIRS have high enough spatial and temporal coverage to monitor persistent polynyas at PIGIS and can distinguish between latent- and sensible-heat polynyas based on the spatial extent, shape, and magnitude of the thermal anomaly. Furthermore, for all months considered, locations where we observed a relatively warm temperature signal in the thermal imagery coincided with warm seal-tag-derived near-surface temperature measurements. Seal-tag data indicated that these anomalously warm wintertime surface ocean temperatures can be used as a proxy for subsurface ocean temperatures, down to 150–200 m depth, rather than solely being representative of ocean-surface processes. These findings suggest that remotely-sensed thermal anomalies near polynyas can be used for monitoring sensible-heat polynya spatial (horizontal and vertical) and thermal structure during polar night. Our results are likely applicable to all warm-cavity ice shelves.

Furthermore, we found that regions of relatively high surface temperature near PIGIS have a high MW content (see Fig. 6), consistent with the ocean properties found in the PIG persistent polynyas in 2014 [13]. The buoyant MW plumes beneath PIG are turbulent and entrain mCDW as they rise; they carry enough heat to drive basal melting and sometimes advect the residual heat (i.e., heat not consumed during ice melt) to the ocean surface and melt openings in the sea ice that we observe from satellites (see [18]). These polynyas therefore provide windows into processes occurring in the subice-shelf environment and directly represent the integrated interactions of mCDW with the ice-shelf base from the grounding zone to the ice front. The potential for continuous high-resolution monitoring of sensible-heat polynya thermal structure and variability provides a unique opportunity to identify and track the thermal signature of these polynyas in wintertime at PIGIS and elsewhere on the Antarctic coast in regions with similar hydrographic conditions.

B. Unique Potential of TIRS

The finer spatial resolution (100 m) of Landsat 8 wintertime thermal imagery captures detailed structural variability within these polynyas [see Fig. 3 (left column)], which may provide deeper insight into subice-shelf processes during polar night if this dataset is collected operationally. Additionally, this fine resolution imagery may result in more reliable polynya

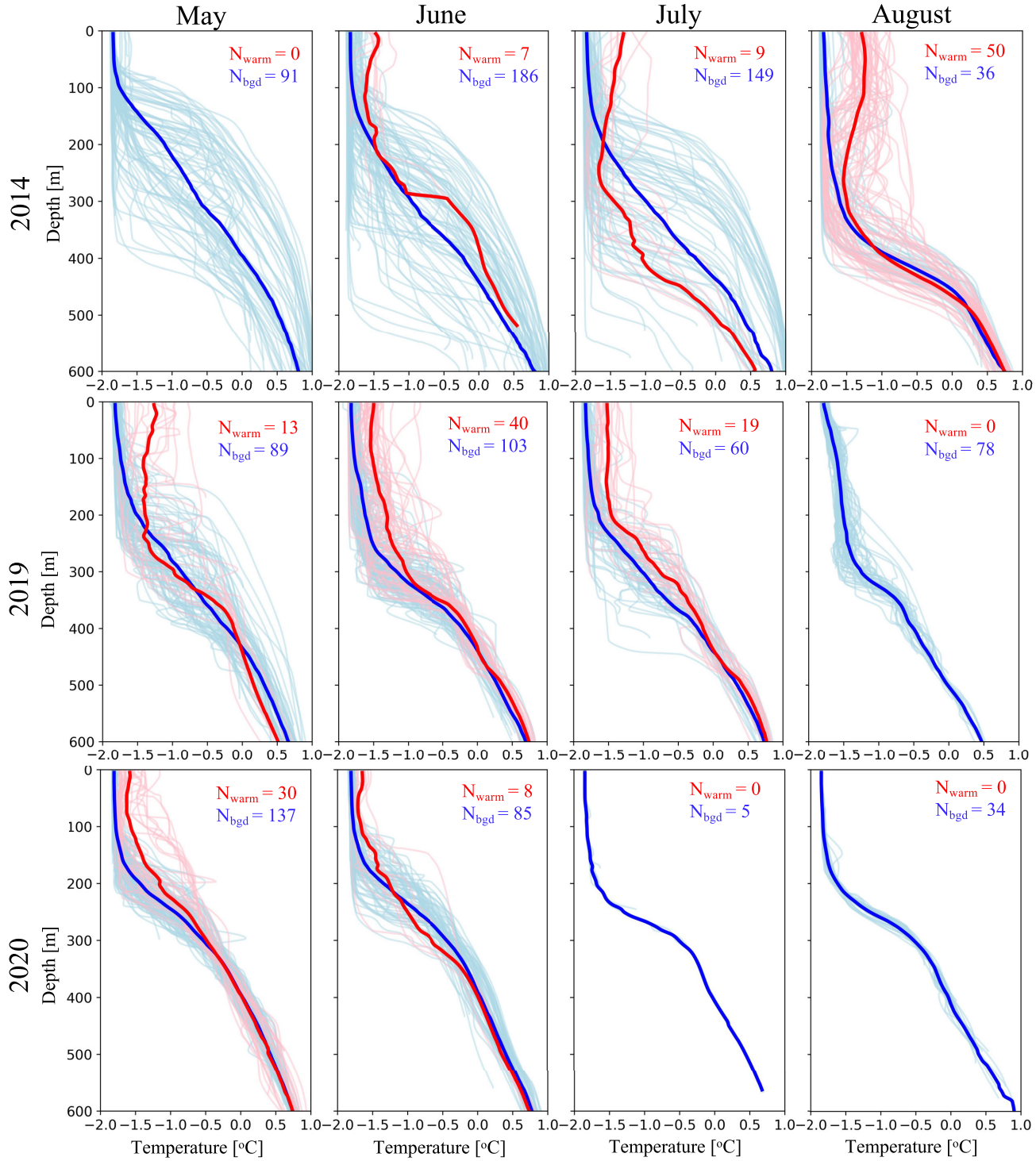

Fig. 5. Seal-tag-derived temperature profiles near PIGIS front. In all months where there are multiple warm profiles near the ice front, the warm surface temperature anomaly extended down to ~400 m depth. Blue and red lines represent background (bgd) and warm temperature profiles, respectively, with the corresponding bold lines representing the monthly means for each. N_{warm} and N_{bgd} indicate the monthly warm and background profile count near PIGIS (see Fig. 1, orange box).

absolute surface temperature retrievals than currently available with MODIS. The thermal structure of the polynya signal at the surface can help identify where plume thermal advection and/or basal channel outflow may be strongest, among other influencing factors [16], [18]. In May 2019, and consistent with published literature, we observed a concentration of warm water near the western shear margin of PIG, where strong basal channel outflow has previously been identified [16], [18] from both Landsat and MODIS thermal imagery. However, temperature gradients and plume edges are more distinct in Landsat TIRS, illustrating its potential use in long-term investigations of polynya thermal structure.

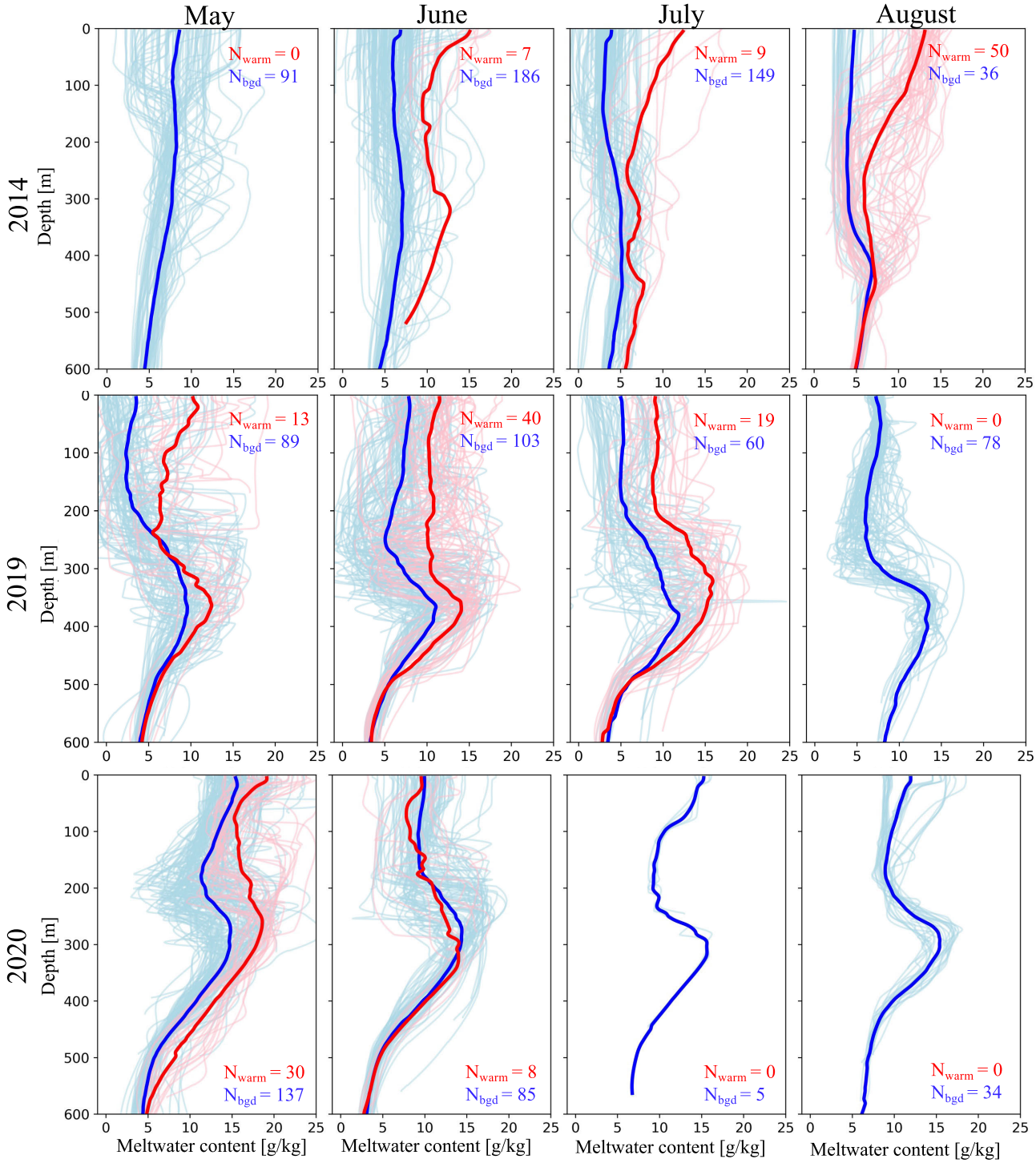

Fig. 6. Seal-tag-derived MW profiles near PIGIS front. In all months where there are multiple warm profiles (N_{warm} = 7–50) near the ice front, warm profiles corresponded to greater MW content than background (bgd) dives. Seal-tag-derived potential density profiles can be found in the Supplementary Material (see Fig. S3).

C. MODIS and TIRS Limitations

Although satellite thermal detectors provide near-continuous polynya detection capabilities in wintertime at PIG, some TIRS, MODIS, and seal-tag CTD instrumental constraints provide barriers to building a direct proxy between remotely sensed temperatures and surface ocean temperatures. We found that MODIS-derived wintertime surface ocean temperatures near PIGIS did not strongly correlate with seal-derived surface temperatures (see Fig. 8). The absence of a correlation between both surface temperature measurements may be largely attributed to the coarse spatial resolution of MODIS (1 km), meaning that surface temperatures are integrated over too large an area in PIG's complex coastal margin to provide a

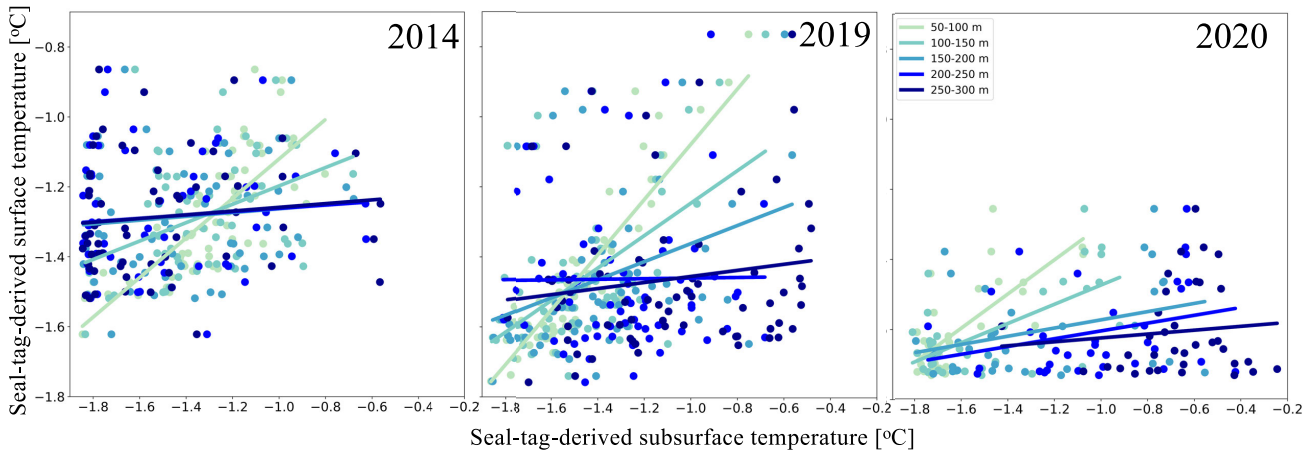

Fig. 7. 2014, 2019, and 2020 seal-derived surface-subsurface water-column correlations for warm profiles. Subsurface temperatures were averaged over 50-m depth intervals (50–100, 100–150, 150–200, 200–250, and 250–300 m) and correlated with mean surface (0–50 m) temperatures. The equivalent figure for background profiles can be found in the Supplementary Material (see Fig. S4).

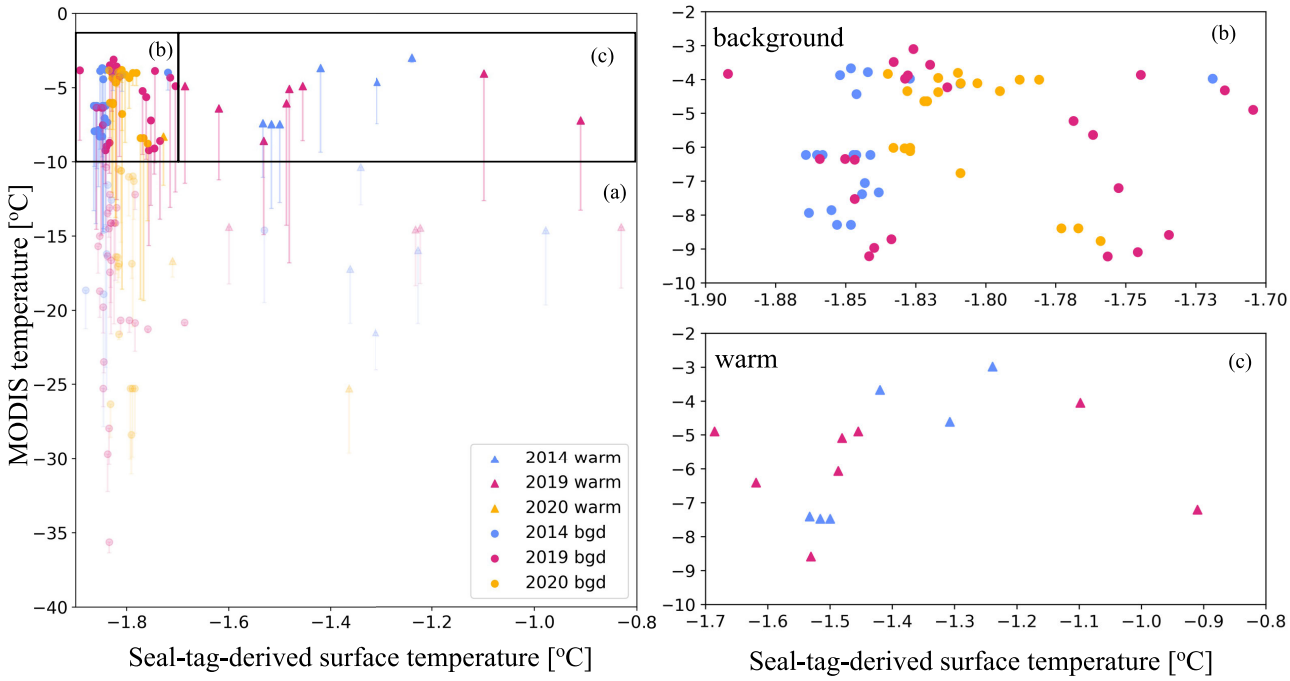

Fig. 8. (a) Extracted MODIS temperatures compared to seal-tag-derived surface temperatures for all 67 data pairs near the PIGIS. Vertical bars show the range of MODIS temperatures within 6 km of each seal-tag location, with markers indicating the maximum value [triangles for warm profiles; circles for background (bgd) profiles]. The transparency threshold set at −10 °C indicates the threshold above which the extracted MODIS surface temperatures likely reflect temperatures of open ocean and/or thin sea ice and below which likely reflect thicker sea ice and/or clouds. MODIS- and seal-tag-derived surface temperatures for (b) background and (c) warm profiles are highlighted panels of boxes shown in (a).

meaningful estimate of ocean thermal properties. Instead these observations likely reflect an average temperature observation from a mixed pixel (e.g., any combination of cloud, grease ice, pancake ice, thick sea ice, part of the calving front, open ocean), resulting in a "cold bias." Such "cold bias" has been demonstrated in the Arctic (see [34]), but until now had not been shown in the southern high latitudes. This issue may be overcome by applying subpixel retrieval methods, such as spectral unmixing or multisensor data fusion (see [49], [50]), which may be able to separate the thermal contributions of each constituent to the infrared emissions of the larger pixel. Although TIRS measurements have a much higher spatial resolution, there is no calibrated Landsat sea surface temperature product for Antarctica [38]. Hence, we cannot assess TIRS measurements of polynya thermal structure and instead can only discuss relative differences in brightness temperature. Additionally, some of the observed inconsistencies between datasets may arise in part due to seal-tag positioning errors, which have been estimated to be ∼4 km (see [51]). Furthermore, even when measurements are taken at the same location in the ocean, discrepancies between surface temperature measurements from seal-tag and MODIS datasets may occur due to large temporal variability on subdaily timescales [see Fig. 3 (top row)] caused by

rapid wintertime surface cooling, frazil sea ice formation, fast surface currents, advection and obscuration by nearly transparent clouds, and intense wind stirring.

D. Future Use of Thermal Imagery for Sensible-Heat Polynya Monitoring

By linking MODIS and TIRS thermal data to seal-tag measurements we show that we can monitor thermal variations from space, year-round, at high temporal resolution. However, only MODIS currently captures images year-round in polar regions and few of these images are processed into the MOD/MYD09 datasets (due to errors arising from cloud shadow, high aerosol content, high view angle, or high solar zenith angle; see [35]). Further, as a result of its coarse spatial resolution, MODIS cannot resolve the persistent polynyas around Antarctica that are smaller than those at PIG. Landsat 8 and the recently launched Landsat 9 have the spatial resolution to detect these small polynyas, but only acquire images during polar winter if special acquisitions are requested for specific image tiles, leaving most of the rest of Antarctica—including small polynyas—unobserved during wintertime. Consistent high spatial and temporal resolution wintertime thermal imagery of the poles would provide invaluable insight for tracking ice–ocean interactions and changes. Such data would reduce how heavily we currently rely on the scarce ocean record in the critical Amundsen Sea sector of Antarctica (see [52]). Therefore, we recommend that Landsat 8/9 and future missions with high spatial resolution and high radiometric fidelity thermal instruments begin operational wintertime thermal data collection at the high latitudes, particularly in the complex and dynamic coastal margins.

Access to high-resolution wintertime thermal imagery would allow not only continuous monitoring of sensible-heat polynyas, but also characterization of subsurface mixed layer temperature in regions where we observe sensible-heat polynyas. The correlation depth between surface (polynya) and subsurface (plume) anomalously warm temperatures (found here to be down to 150 m depth) is strongest in the winter, where a homogenous mixed layer allows plumes to more frequently rise to the surface, relative to summertime [13]. These seasonally controlled dynamic processes hence allow us to fill the gap of the year-round sensible-heat polynya monitoring by inferring subsurface temperature conditions from remote sensing observations in winter.

V. Summary

Sensible-heat polynyas appear near many ice shelves in the Amundsen Sea, but we have limited wintertime observations of how these polynyas evolve and interact with ice shelves. Here, we linked wintertime thermal remote sensing from MODIS and TIRS with unique in situ seal-tag hydrographic measurements to investigate the spatiotemporal, vertical, and thermal structural variability of sensible-heat polynyas near PIGIS. Pairing these independent observations, we presented the first study that combines wintertime remote sensing and seal-borne observations to investigate polynya processes in Antarctica.

Our work demonstrates that MODIS thermal anomalies can be used to monitor polynya thermal structure and polynya processes during polar night; this finding becomes particularly important when we have limited access to ocean records, as is often the case in Antarctica. Both MODIS and TIRS provide high enough spatial and temporal coverage of polynyas to be used to distinguish between latent- and sensible-heat polynyas based on the spatial extent, shape, and magnitude of the thermal anomaly. Furthermore, we show that the finer spatial resolution of Landsat 8 wintertime thermal imagery captures structural thermal variability within these polynyas in greater detail than MODIS; this fine-scale mapping may provide insight into plume dynamics and subice-shelf processes during polar night if this dataset is collected operationally and can be developed into a calibrated sea surface temperature product. Access to calibrated surface temperatures from Landsat 8 would likely yield a better correlation between seal-borne and space-borne surface temperatures at PIG; this could allow for wintertime characterization of subsurface ocean temperatures down to 150–200 m depth (above which depth near-surface ocean temperatures remain correlated through the subsurface) near PIGIS, from remote sensing observations alone. This MODIS and TIRS pilot study therefore shows promise that high spatial resolution ocean thermal measurements can be used for year-round monitoring of polynya, ice-front, and subice-shelf processes in Antarctica. Our analysis broadens our limited understanding of wintertime ice-ocean processes in this region, where most of our current observations are from summertime, and where ice shelves are particularly vulnerable to ocean-driven changes.

Acknowledgment

Logistical support for data collection was provided by NSF-U.S. Antarctic Program and NERC-British Antarctic Survey. ITGC Contribution No. ITGC-089. The data (https://doi.org/10.5281/zenodo.7696898) and code (https://doi.org/10.5281/zenodo.7843547) that support the findings of this study are openly available. We would also like to thank the editor and anonymous reviewers, whose comments improved the manuscript.

References

[1] J. Mouginot, E. Rignot, and B. Scheuchl, "Sustained increase in ice discharge from the Amundsen Sea Embayment, West Antarctica, from 1973 to 2013," *Geophys. Res. Lett.*, vol. 41, no. 5, pp. 1576–1584, Mar. 2014.

[2] E. Rignot, J. Mouginot, M. Morlighem, H. Seroussi, and B. Scheuchl, "Widespread, rapid grounding line retreat of Pine Island, Thwaites, Smith, and Kohler glaciers, West Antarctica, from 1992 to 2011," *Geophys. Res. Lett.*, vol. 41, no. 10, pp. 3502–3509, May 2014.

[3] A. Shepherd, D. J. Wingham, J. A. D. Mansley, and H. F. J. Corr, "Inland thinning of Pine Island Glacier, West Antarctica," *Science*, vol. 291, no. 5505, pp. 862–864, Feb. 2001.

[4] B. Smith et al., "Pervasive ice sheet mass loss reflects competing ocean and atmosphere processes," *Science*, vol. 368, no. 6496, pp. 1239–1242, Jun. 2020.

[5] K. Christianson et al., "Sensitivity of Pine Island Glacier to observed ocean forcing," *Geophys. Res. Lett.*, vol. 43, no. 20, pp. 1–9, Oct. 2016.

[6] S. S. Jacobs, H. H. Hellmer, and A. Jenkins, "Antarctic ice sheet melting in the Southeast Pacific," *Geophys. Res. Lett.*, vol. 23, no. 9, pp. 957–960, May 1996.

[7] S. S. Jacobs, A. Jenkins, C. F. Giulivi, and P. Dutrieux, "Stronger ocean circulation and increased melting under Pine Island Glacier ice shelf," *Nature Geosci.*, vol. 4, no. 8, pp. 519–523, Aug. 2011.

[8] P. Dutrieux et al., "Strong sensitivity of Pine Island ice-shelf melting to climatic variability," *Science*, vol. 343, no. 6167, pp. 174–178, Jan. 2014.

[9] A. K. Wåhlin et al., "Pathways and modification of warm water flowing beneath Thwaites Ice Shelf, West Antarctica," *Sci. Adv.*, vol. 7, no. 15, pp. 1–15, Apr. 2021.

[10] A. K. Wåhlin, X. Yuan, G. Björk, and C. Nohr, "Inflow of warm circumpolar deep water in the central Amundsen shelf," *J. Phys. Oceanogr.*, vol. 40, no. 6, pp. 1427–1434, Jun. 2010.

[11] A. Jenkins et al., "Observations beneath Pine Island Glacier in West Antarctica and implications for its retreat," *Nature Geosci.*, vol. 3, no. 7, pp. 468–472, Jul. 2010.

[12] P. E. D. Davis et al., "Variability in basal melting beneath Pine Island Ice Shelf on weekly to monthly timescales," *J. Geophys. Res., Oceans*, vol. 123, no. 11, pp. 8655–8669, Nov. 2018.

[13] Y. Zheng et al., "Winter seal-based observations reveal glacial meltwater surfacing in the southeastern Amundsen Sea," *Commun. Earth Environ.*, vol. 2, no. 1, pp. 1–9, Mar. 2021.

[14] K. Heywood et al., "Between the devil and the deep blue sea: The role of the Amundsen Sea continental shelf in exchanges between ocean and ice shelves," *Oceanography*, vol. 29, no. 4, pp. 118–129, Dec. 2016.

[15] A. C. N. Garabato et al., "Vigorous lateral export of the meltwater outflow from beneath an Antarctic ice shelf," *Nature*, vol. 542, no. 7640, pp. 219–222, Feb. 2017.

[16] K. E. Alley, T. A. Scambos, M. R. Siegfried, and H. A. Fricker, "Impacts of warm water on Antarctic ice shelf stability through basal channel formation," *Nature Geosci.*, vol. 9, no. 4, pp. 290–293, Apr. 2016.

[17] K. E. Alley, T. A. Scambos, R. B. Alley, and N. Holschuh, "Troughs developed in ice-stream shear margins precondition ice shelves for ocean-driven breakup," *Sci. Adv.*, vol. 5, no. 10, Oct. 2019, Art. no. eaax2215.

[18] K. D. Mankoff, S. S. Jacobs, S. M. Tulaczyk, and S. E. Stammerjohn, "The role of Pine Island Glacier ice shelf basal channels in deep-water upwelling, Polynyas and ocean circulation in Pine Island Bay, Antarctica," *Ann. Glaciol.*, vol. 53, no. 60, pp. 123–128, 2012.

[19] P. S. Anderson, "Evidence for an Antarctic winter coastal Polynya," *Antarctic Sci.*, vol. 5, no. 2, pp. 221–226, Jun. 1993.

[20] T. Millgate, P. R. Holland, A. Jenkins, and H. L. Johnson, "The effect of basal channels on oceanic ice-shelf melting," *J. Geophys. Res., Oceans*, vol. 118, no. 12, pp. 6951–6964, Dec. 2013.

[21] C. V. Gladish, D. M. Holland, P. R. Holland, and S. F. Price, "Ice-shelf basal channels in a coupled ice/ocean model," *J. Glaciol.*, vol. 58, no. 212, pp. 1227–1244, 2012.

[22] C. F. Dow et al., "Basal channels drive active surface hydrology and transverse ice shelf fracture," *Sci. Adv.*, vol. 4, no. 6, Jun. 2018, Art. no. eaao7212.

[23] F. Arce et al., "Elephant seal foraging success is enhanced in Antarctic coastal Polynyas," *Proc. Roy. Soc. B, Biol. Sci.*, vol. 289, no. 1967, Jan. 2022, Art. no. 20212452.

[24] P. Yager et al., "A carbon budget for the Amundsen Sea Polynya, Antarctica: Estimating net community production and export in a highly productive polar ecosystem," *Elementa, Sci. Anthropocene*, vol. 4, Jan. 2016.

[25] M. A. Morales Maqueda, A. J. Willmott, and N. R. T. Biggs, "Polynya dynamics: A review of observations and modeling," *Rev. Geophy.*, vol. 42, no. 1, pp. 1–13, Mar. 2004.

[26] H. B. DeJong, R. B. Dunbar, and E. A. Lyons, "Late summer frazil ice-associated algal blooms around Antarctica," *Geophys. Res. Lett.*, vol. 45, no. 2, pp. 826–833, Jan. 2018.

[27] G. Aulicino et al., "A new approach for monitoring the Terra Nova Bay Polynya through MODIS ice surface temperature imagery and its validation during 2010 and 2011 winter seasons," *Remote Sens.*, vol. 10, no. 3, p. 366, Feb. 2018.

[28] A. Ciappa, L. Pietranera, and G. Budillon, "Observations of the Terra Nova Bay (Antarctica) Polynya by MODIS ice surface temperature imagery from 2005 to 2010," *Remote Sens. Environ.*, vol. 119, pp. 158–172, Apr. 2012.

[29] T. Markus and B. A. Burns, "Detection of coastal Polynyas with passive microwave data," *Ann. Glaciol.*, vol. 17, pp. 351–355, Jan. 1993.

[30] R. A. Massom, K. L. Hill, V. I. Lytle, A. P. Worby, M. J. Paget, and I. Allison, "Effects of regional fast-ice and iceberg distributions on the behaviour of the Mertz Glacier Polynya, East Antarctica," *Ann. Glaciol.*, vol. 33, pp. 391–398, Jan. 2001.

[31] W. N. Meier, F. Fetterer, J. S. Stewart, and S. Helfrich, "How do sea-ice concentrations from operational data compare with passive microwave estimates? Implications for improved model evaluations and forecasting," *Ann. Glaciol.*, vol. 56, no. 69, pp. 332–340, 2015.

[32] R. Bindschadler, D. G. Vaughan, and P. Vornberger, "Variability of basal melt beneath the Pine Island Glacier ice shelf, West Antarctica," *J. Glaciol.*, vol. 57, no. 204, pp. 581–595, 2011.

[33] C. J. Merchant, "Thermal remote sensing of sea surface temperature," in *Thermal Infrared Remote Sensing*. Cham, Switzerland: Springer, 2013, pp. 287–313.

[34] C. Jia and P. J. Minnett, "High latitude sea surface temperatures derived from MODIS infrared measurements," *Remote Sens. Environ.*, vol. 251, Dec. 2020, Art. no. 112094.

[35] E. Vermote, J. Roger, and J. Ray, "MODIS surface reflectance user's guide collection 6, version 1.4, May 2015," MODIS Land Surf. Reflectance Sci. Comput. Facility, Tech. Rep. Collection 6, Version 1.4, 2018.

[36] S. A. Ackerman, K. I. Strabala, W. P. Menzel, R. A. Frey, C. C. Moeller, and L. E. Gumley, "Discriminating clear sky from clouds with MODIS," *J. Geophys. Res., Atmos.*, vol. 103, no. D24, pp. 32141–32157, Dec. 1998.

[37] K. A. Kilpatrick, G. Podestá, E. Williams, S. Walsh, and P. J. Minnett, "Alternating decision trees for cloud masking in MODIS and VIIRS NASA sea surface temperature products," *J. Atmos. Ocean. Technol.*, vol. 36, no. 3, pp. 387–407, Mar. 2019.

[38] K. Bradtke, "Landsat 8 data as a source of high resolution sea surface temperature maps in the Baltic sea," *Remote Sens.*, vol. 13, no. 22, p. 4619, Nov. 2021.

[39] A. Treasure et al., "Marine mammals exploring the oceans pole to pole: A review of the MEOP consortium," *Oceanography*, vol. 30, no. 2, pp. 132–138, Jun. 2017.

[40] L. Boehme et al., "Technical note: Animal-borne CTD-satellite relay data loggers for real-time oceanographic data collection," *Ocean Sci.*, vol. 5, no. 4, pp. 685–695, Dec. 2009.

[41] M. Fedak, "Overcoming the constraints of long range radio telemetry from animals: Getting more useful data from smaller packages," *Integrative Comparative Biol.*, vol. 42, no. 1, pp. 3–10, Feb. 2002.

[42] T. J. McDougall and P. M. Barker, "Getting started with TEOS-10 and the Gibbs seawater (GSW) oceanographic toolbox," in *Proc. SCOR/IAPSO WG*, vol. 127, 2011, pp. 1–28.

[43] L. Boehme and I. Rosso, "Classifying oceanographic structures in the Amundsen Sea, Antarctica," *Geophys. Res. Lett.*, vol. 48, no. 5, Mar. 2021, Art. no. e2020GL089412.

[44] L. C. Biddle, B. Loose, and K. J. Heywood, "Upper ocean distribution of glacial meltwater in the Amundsen Sea, Antarctica," *J. Geophys. Res., Oceans*, vol. 124, no. 10, pp. 6854–6870, Oct. 2019.

[45] D. A. Sutherland, F. Straneo, G. B. Stenson, F. J. M. Davidson, M. O. Hammill, and A. Rosing-Asvid, "Atlantic water variability on the SE Greenland continental shelf and its relationship to SST and bathymetry," *J. Geophys. Res., Oceans*, vol. 118, no. 2, pp. 847–855, Feb. 2013.

[46] L. Gerrish, P. Fretwell, and P. Cooper, "High resolution vector polygons of the Antarctic coastline (7.4)," U.K. polar data centre, Natural Environment Research Council, U.K. Research and Innovation, Tech. Rep., 2021.

[47] A. M. Thurnherr, S. S. Jacobs, P. Dutrieux, and C. F. Giulivi, "Export and circulation of ice cavity water in Pine Island bay, West Antarctica," *J. Geophys. Res., Oceans*, vol. 119, no. 3, pp. 1754–1764, Mar. 2014.

[48] P. Wadhams, G. Aulicino, F. Parmiggiani, P. O. G. Persson, and B. Holt, "Pancake ice thickness mapping in the Beaufort sea from wave dispersion observed in SAR imagery," *J. Geophys. Res., Oceans*, vol. 123, no. 3, pp. 2213–2237, Mar. 2018.

[49] T. Markus and B. A. Burns, "A method to estimate subpixel-scale coastal Polynyas with satellite passive microwave data," *J. Geophys. Res.*, vol. 100, no. C3, pp. 4473–4487, Mar. 1995.

[50] A. Preußer, G. Heinemann, S. Willmes, and S. Paul, "Multi-decadal variability of Polynya characteristics and ice production in the North Water Polynya by means of passive microwave and thermal infrared satellite imagery," *Remote Sens.*, vol. 7, no. 12, pp. 15844–15867, Nov. 2015.

[51] L. Padman et al., "Oceanic controls on the mass balance of Wilkins Ice Shelf, Antarctica," *J. Geophys. Res., Oceans*, vol. 117, no. C1, pp. 1–10, Jan. 2012.

[52] T. A. Scambos et al., "How much, how fast? A science review and outlook for research on the instability of Antarctica's Thwaites Glacier in the 21st century," *Global Planet. Change*, vol. 153, pp. 16–34, Jun. 2017.

Elena Savidge received the B.S. degree (Hons.) in Earth and ocean science from the University of Victoria, Victoria, BC, Canada, in 2020. She is currently pursuing the Ph.D. degree in geophysics with the Colorado School of Mines, Golden, CO, USA, under the supervision of Dr. Matthew R. Siegfried.

As part of the Mines Glaciology Laboratory, she uses thermal and optical imagery combined with hydrographic measurements to study ice-ocean processes in West Antarctica.

Ms. Savidge is a Natural Sciences and Engineering Research Council of Canada Postgraduate Scholarship—Doctoral Fellow.

Tasha Snow received the B.S. degree in oceanography from the University of Washington, Seattle, WA, USA, in 2007, the M.S. degree in marine science from the University of South Florida, Tampa, FL, USA, in 2014, and the Ph.D. degree in geography from the University of Colorado Boulder, Boulder, CO, USA, in 2021.

She is currently a Post-Doctoral Research Associate with the Department of Geophysics, Colorado School of Mines, Golden, CO, USA. Her research interests include using satellite remote sensing with field observations to find new ways of observing glacier–ocean interactions and ocean heat transport around the coastlines of Greenland and Antarctica.

Matthew R. Siegfried (Member, IEEE) received the B.A. and M.S. degrees in Earth sciences from the Dartmouth College, Hanover, NH, USA, in 2008 and 2010, respectively, and the Ph.D. degree in geophysics from the Scripps Institution of Oceanography, University of California at San Diego, La Jolla, CA, USA, in 2015.

He is currently an Assistant Professor with the Department of Geophysics and an Affiliate Faculty Member in hydrologic sciences and engineering and humanitarian engineering with the Colorado School of Mines, Golden, CO, USA. His research group at the Mines Glaciology Laboratory uses satellite remote sensing techniques in combination with field-based and airborne geophysical methods to understand physical processes of the Earth's cryosphere. He participated in the NASA's ICESat-2 mission Science Definition Team and Science Team activities from 2011 to 2020, was a member of the NASA's final Operation IceBridge Science Team from 2017 to 2020, and is currently a member of the NASA's ICESat-2 Science Team and NASA's Decadal Survey Incubation Team.

Yixi Zheng received the B.S. degree in meteorology and oceanography from the University of East Anglia, Norwich, U.K., in 2018, the B.S. degree majoring in physical oceanography and minoring in marine meteorology from the Ocean University of China, Qingdao, China, in 2018, and the Ph.D. degree in physical oceanography from the University of East Anglia in 2022.

She is currently a Post-Doctoral Researcher with the University of East Anglia. Her research interests include all physical-oceanography questions, in particular those regarding the interactions between ocean and ice shelves in Antarctica. She is supported by the China Scholarship Council and the University of East Anglia.

Ana B. Villas Bôas received the B.S. degree in physics from the Federal University of Rio Grande do Norte, Natal, Brazil, in 2011, the M.Sc. degree in physical oceanography from the University of São Paulo, São Paulo, Brazil, in 2014, and the Ph.D. degree in physical oceanography from the Scripps Institution of Oceanography, University of California at San Diego, La Jolla, CA, USA, in 2020.

She is currently an Assistant Professor with the Department of Geophysics, Colorado School of Mines, Golden, CO, USA. Her research interests include modeling, theory, and observation to improve our understanding of how ocean surface gravity waves interact with other processes in the upper-ocean and the overlying atmosphere.

Guilherme (Gui) A. Bortolotto received the B.S. degree in veterinary medicine from the University of Santa Catarina State (UDESC), Lages, Brazil, in 2010, the M.S. degree in zoology from the State University of Santa Cruz (UESC), Ilhéus, Brazil, in 2014, and the Ph.D. degree in biology from the University of St Andrews, St Andrews, U.K., in 2019.

Since 2019, he has been a Post-Doctoral Research Fellow in polar marine ecology with the University of St Andrews. His research interests include statistical ecology and conservation of marine megafauna.

Lars Boehme received the Dipl.Oz. degree in physical oceanography from Kiel University, Kiel, Germany, in 2003, and the Ph.D. degree in oceanography from the University of St Andrews, St Andrews, U.K., in 2008.

He is currently a Reader/Professor with the Scottish Oceans Institute, University of St Andrews. His research interests include polar oceanography, ocean observations, and the development and application of animal-borne instruments in particular.

Karen E. Alley received the B.A. degree in geology from Colgate University, Hamilton, NY, USA, in 2012, and the Ph.D. degree in geological sciences from the University of Colorado Boulder, Boulder, CO, USA, in 2017.

She is currently an Assistant Professor with the Department of Environment and Geography and the Centre for Earth Observation Science, University of Manitoba, Winnipeg, MB, Canada. Her research interests include using remote sensing and field data to study ice–ocean interaction that affecting Antarctica's floating ice shelves and glacier changes in the Baffin Bay region of the Canadian Arctic and Greenland.